Influence of the central mode and soft phonon on the microwave dielectric loss near the strain-induced ferroelectric phase transitions in $Sr_{n+1}Ti_nO_{3n+1}$

Veronica Goian,[1] Stanislav Kamba,[1,*] Nathan Orloff,[2] Turan Birol,[3] Che Hui Lee,[4] Dmitry Nuzhnyy,[1] James C. Booth,[5] Margitta Bernhagen,[6] Reinhard Uecker,[6] and Darrell G. Schlom[4,7]

[1]*Institute of Physics, Academy of Sciences of the Czech Republic, Na Slovance 2, 182 21 Prague 8, Czech Republic*

[2]*Department of Physics, University of Maryland, College Park, Maryland 20742, USA*

[3]*Department of Physics and Astronomy, Rutgers University, Piscataway, New Jersey 08854, USA*

[4]*Department of Materials Science and Engineering, Cornell University, Ithaca, New York 14853, USA*

[5]*National Institute of Standards and Technology, Boulder, Colorado 80305, USA*

[6]*Leibniz Institute for Crystal Growth, Max-Born-Strasse 2, D-12489 Berlin, Germany.*

[7]*Kavli Institute at Cornell for Nanoscale Science, Ithaca, New York 14853, USA*

(Received 12 August 2014; revised manuscript received 12 September 2014; published 12 November 2014)

Recently, Lee *et al.* [Nature (London) **502**, 532 (2013)] used ~1% tensile strain to induce a ferroelectric instability in thin films of $Sr_{n+1}Ti_nO_{3n+1}$ ($n = 1-6$) phases. They showed that the Curie temperature T_C gradually increased with n, reaching 180 K for $Sr_7Ti_6O_{19}$ ($n = 6$). The permittivity of this ($n = 6$) sample could also be tuned significantly by the application of an electric field with exceptionally low dielectric loss at 300 K, rivaling all known tunable microwave dielectrics. Here, we present microwave (MW), terahertz, and infrared spectra of strained $Sr_{n+1}Ti_nO_{3n+1}$ thin films deposited on (110) $DyScO_3$. Near the ferroelectric phase transitions, we observe the splitting and shifting of phonon and central mode frequencies, demonstrating the change of crystal symmetry below T_C. Moreover, our spectra reveal that the central mode contribution dominates MW loss. In the $Sr_7Ti_6O_{19}$ thin film, the central mode vanishes at 300 K, explaining its low MW loss. Finally, we discuss the origin and general conditions for the appearance of central modes near ferroelectric phase transitions.

DOI: 10.1103/PhysRevB.90.174105 PACS number(s): 63.20.−e, 77.22.Gm, 77.55.F−, 68.35.Rh

I. INTRODUCTION

The long-lasting quest for low-loss and highly tunable dielectric materials is the focus of much of the research on microwave (MW) dielectric materials [1,2]. High tunability of the dielectric permittivity (ε') under the application of an electric field is usually obtained near ferroelectric (FE) phase transitions, where ε' is very high. Unfortunately, FEs frequently have high dielectric loss in the MW region, which is often attributed to the thermal vibrations of FE domain walls. For that reason, FE materials are actually used in the paraelectric state at temperatures that are just above the Curie temperature T_C. Arguably one of the most useful and commonly used tunable dielectrics is $Ba_{1-x}Sr_xTiO_3$, which is popular because its T_C can be easily tuned by chemical substitution of Ba with Sr. This unique ability enables material scientists to alter its T_C from 390 K down to 0 K [3]. The electric tunability of ε' in $Ba_{1-x}Sr_xTiO_3$ is relatively high (nearly 80% in some reports [4]), but the dielectric loss is unfortunately also rather high at frequencies above 10 GHz [5,6] due to the large anharmonicity of its crystal lattice [7]. For this reason, the search for new highly tunable MW materials with low loss continues.

The Ruddlesden-Popper (RP) crystal structure has the general chemical formula $A_{n+1}B_nO_{3n+1}$, $n = 1,2,3...\infty$. Along the [001] direction, it consists of n perovskite blocks separated and crystallographically sheared by $(AO)_2$ layers [8,9] [see Fig. 1(a)]. As shown in several reports [10,11], the $Sr_{n+1}Ti_nO_{3n+1}$ series is of particular interest. Notably, the parameter n enables the value of ε' in $Sr_{n+1}Ti_nO_{3n+1}$ to be tuned in ceramics [10] and thin films [12]. At room temperature, the relative ε' increases from 37 (for $n = 1$) to 100 (for $n = 4$) [10]. On cooling, ε' and its temperature dependence increases with the parameter n, but no FE phase transition has been observed even down to liquid helium temperatures [11,12]. Interestingly, the permittivity exhibits no frequency dispersion in the MW region [11,12]; therefore, $Sr_{n+1}Ti_nO_{3n+1}$ ceramics and unstrained films exhibit low dielectric loss, making them attractive for low-temperature MW devices [13]. The $n = \infty$ end member of the RP series, bulk $SrTiO_3$, has $\varepsilon' = 290$ at 300 K. $SrTiO_3$ is perhaps the best-known quantum paraelectric material, where ε' increases on cooling, saturating at ~25 000 below 10 K [14]. The tunability of $SrTiO_3$ becomes large only at low temperatures where the ε' is high. This begs the questions: (1) how can the operating temperature of these highly tunable dielectrics be shifted to the room temperature without significantly increasing the dielectric losses? And (2) what is the controlling mechanism that we can employ to tune the operating temperatures above 300 K?

It is well known that ε' can be enhanced with suitable epitaxial tensile strain in $SrTiO_3$ thin films. In fact, 1% tensile strain can even induce the ferroelectricity near 270 K in 50-nm-thick $SrTiO_3$ thin films deposited on (110) $DyScO_3$ substrates [15]. The ε' of such films can be significantly tuned by an applied electric field at kilohertz (kHz), MW [15], and terahertz (THz) [16] frequencies, because the soft mode (SM) frequency is sensitive to external electric field [16]. Nevertheless, MW dielectric loss of strained $SrTiO_3$ thin films at room temperature is comparable to $Ba_{1-x}Sr_xTiO_3$ ceramics [15]. Kadlec *et al.* [16] have attributed these losses to a central mode (i.e., dielectric relaxation below the phonon frequencies, abbreviation CM) that arises in the dielectric

*Corresponding author: kamba@fzu.cz

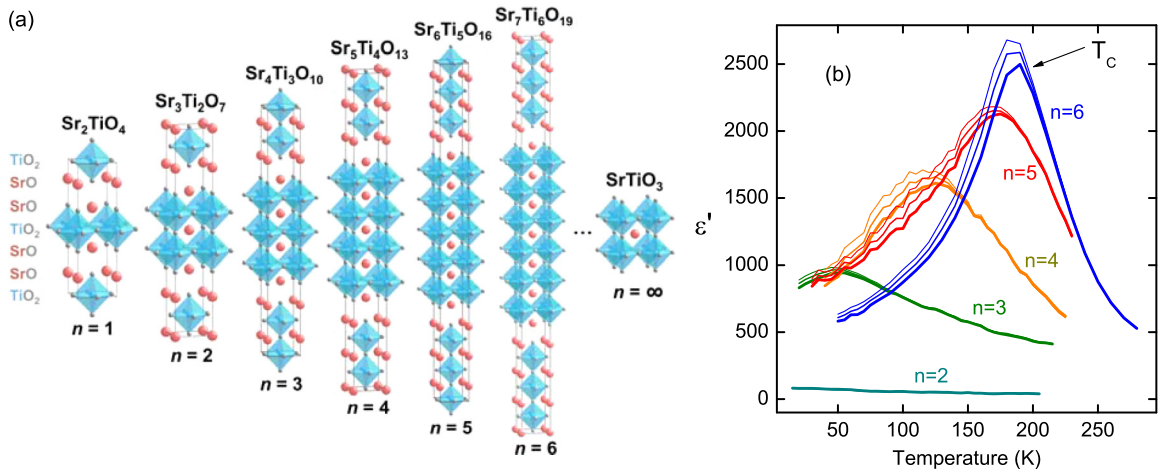

FIG. 1. (Color online) (a) Schematic of the crystal structure of a unit cell of the $n = 1$–6 and $n = \infty$ members of the $Sr_{n+1}Ti_nO_{3n+1}$ homologous series. (b) Temperature dependence of in-plane dielectric permittivity of $n = 2$–6 films at 10 kHz (the thinnest line), 100 kHz, and 1 MHz (the thickest line; modified from Ref. [18]).

spectra of $SrTiO_3$ thin films as the material approaches temperatures close to the FE phase transition. The CM is usually infrared (IR) inactive far above T_C (i.e. its dielectric strength $\Delta\varepsilon_{CM} = 0$), but it becomes IR active (i.e. $\Delta\varepsilon_{CM} \neq 0$) near T_C due to its linear coupling with the polar SM when the SM frequency becomes close to the CM frequency [16]. The SM practically partially transfers its dielectric strength $\Delta\varepsilon_{SM}$ to the CM (therefore $\Delta\varepsilon_{CM} \neq 0$), and because the CM is the lowest frequency polar excitation, it significantly enhances both ε' and dielectric loss ε'' in the MW region. The electric field increases the SM frequency, consequently reducing $\Delta\varepsilon_{SM}$ and $\Delta\varepsilon_{CM}$ and therefore reducing ε' and ε'' at MW and THz frequencies [16].

Recently, first principles calculations [17] of $Sr_{n+1}Ti_nO_{3n+1}$ predicted a FE phase transition under biaxial tensile strain. Birol *et al.* [17] also found that the instability of the lowest frequency polar phonon (i.e. FE SM) should increase with the strain and with the parameter n expressing the number of $SrTiO_3$ perovskite layers between the $(SrO)_2$ planes. These predictions were then experimentally confirmed by Lee *et al.* [18] for tensile strained $Sr_{n+1}Ti_nO_{3n+1}$ thin films grown on (110) $DyScO_3$ and (110) $GdScO_3$ substrates. Dielectric anomalies consistent with FE phase transitions occurred for $n \geq 3$ [see peaks in $\varepsilon'(T)$ in Fig. 1(b)] [18]. In agreement with theory [17], the experiment revealed that T_C increased with both strain and parameter n [18].

Since the FE phase transition temperature is dramatically increased by tensile strain, ε' of $Sr_{n+1}Ti_nO_{3n+1}$ at room temperature is much higher than that of bulk $Sr_{n+1}Ti_nO_{3n+1}$ ceramics and unstrained thin films. As a result, the tunability $\frac{\varepsilon'(E=0)-\varepsilon'(E)}{\varepsilon'(E=0)}$ of these films by electric field E is also very high. Unlike $Ba_{1-x}Sr_xTiO_3$ ceramics, the MW dielectric loss, $\tan\delta$, of $Sr_7Ti_6O_{19}$ ($n = 6$) thin films was very low at room temperature [18]. Hence, the figure of merit (tunability divided by $\tan\delta$) was an order of magnitude higher than in the best $Ba_{1-x}Sr_xTiO_3$ films. In this paper, we demonstrate that only polar phonons contribute to the MW dielectric loss in the strained $Sr_7Ti_6O_{19}$ thin film at room temperature. At low temperatures, the crystal lattice is more anharmonic due to the presence of lattice instability near 180 K. Within this regime, a CM appears in THz dielectric spectra, enhancing the MW dielectric loss on approaching T_C, but rapidly collapses above 275 K. As a consequence, the CM does not enhance the dielectric loss at room temperature, at least for strained $Sr_7Ti_6O_{19}$. This curiosity—which is a unique property of the strained $Sr_7Ti_6O_{19}$ thin film—will be a central focus of this paper.

All strained $Sr_{n+1}Ti_nO_{3n+1}$ ($n \geqslant 3$) thin films exhibit dielectric dispersion close to temperatures T_m, where the peaks in $\varepsilon'(T)$ develop, and it is reminiscent of relaxor FE behavior. In this paper, we also show that polar phonons, seen in far IR spectra, split near T_C. This is evidence of a structural phase transition in the thin films. Our spectroscopic data together with published second harmonic generation (SHG) measurements and FE hysteresis loops [18] provide evidence that the strained $Sr_{n+1}Ti_nO_{3n+1}$ thin films with $n \geqslant 3$ are not relaxor FEs, but really macroscopically FE at low temperatures.

II. EXPERIMENTAL AND CALCULATION DETAILS

The strained $Sr_{n+1}Ti_nO_{3n+1}$ ($n = 1$–6) films were grown in Veeco Gen10 and 930 oxide molecular-beam epitaxy systems on (110) $DyScO_3$ single crystalline substrates [19]. Molecular beams of strontium and titanium were generated using a low-temperature effusion cell and a Ti-Ball, respectively [20]. The fluxes of both elements were roughly calibrated with a quartz crystal microbalance. A more accurate flux calibration was then achieved using shuttered reflection high-energy electron diffraction (RHEED) intensity oscillations [21]. The ratio between strontium and titanium doses was set to 1:1 by adjusting their durations until the maxima and minima of the shuttered RHEED oscillations neither grew nor diminished in intensity. Once this ratio was correct, the absolute quantity of atoms deposited in each shuttered dose was adjusted to one monolayer of SrO and one monolayer of TiO_2 by monitoring for and avoiding a beat frequency in the shuttered RHEED

oscillation envelope. To grow $Sr_{n+1}Ti_nO_{3n+1}$ phases, both the stoichiometry and each monolayer absolute dose cannot be incorrect by more than about 1%. Each of the members in this series has different sequences of SrO and TiO_2 layers. The strontium and titanium molecular beams were shuttered to match the layering sequence of the desired (001)-oriented $Sr_{n+1}Ti_nO_{3n+1}$ phases.

The IR reflectivity measurements were performed using a Bruker IFS 113v Fourier transform IR spectrometer equipped with a helium-cooled (1.6 K) silicon bolometer. The reflectivity measurements were performed in near normal incidence polarized light. Strained $Sr_{n+1}Ti_nO_{3n+1}$ $(n = 1-6)/DyScO_3$ samples 50 nm thick and a bare (110) $DyScO_3$ substrate were measured in two polarizations ($\boldsymbol{E} \parallel [001]$ and $\boldsymbol{E} \parallel [1\bar{1}0]$ with respect to the (110) $DyScO_3$ substrate) under the same conditions on cooling to 10 K in an Optistat CF cryostat (Oxford Instruments). The 3-mm-thick polyethylene windows used in this measurement were IR transparent only up to 650 cm^{-1}. Room temperature spectra were taken up to 4000 cm^{-1}.

To evaluate the IR reflectance spectra, a model corresponding to a two-layer optical system was used [22]. We first fit the IR reflectivity spectra of the bare substrate at various temperatures. In our experiment, the reflectivity $R(\omega)$ is related to the complex dielectric function $\varepsilon^*(\omega)$ by

$$R(\omega) = \left| \frac{\sqrt{\varepsilon^*(\omega)} - 1}{\sqrt{\varepsilon^*(\omega)} + 1} \right|^2. \quad (1)$$

The complex permittivity $\varepsilon^*(\omega)$ is described by a generalized, factorized damped harmonic oscillator model [23]

$$\varepsilon^*(\omega) = \varepsilon_\infty \prod_j \frac{\omega_{LOj}^2 - \omega^2 + i\omega\gamma_{LOj}}{\omega_{TOj}^2 - \omega^2 + i\omega\gamma_{TOj}}, \quad (2)$$

where ω_{TOj} and ω_{LOj} are the frequencies of jth transverse optic (TO) and longitudinal optic (LO) phonons, and γ_{TOj} and γ_{LOj} are corresponding damping constants. Here, ε_∞ is the high-frequency (electronic) contribution to the permittivity, determined from the room-temperature frequency-independent reflectivity tail above the phonon frequencies. The temperature dependence of ε_∞ was neglected, consistent with its behavior in other related perovskite dielectrics [24]. The parameters (ω_{TOj}, ω_{LOj}, γ_{TOj}, γ_{LOj}, and ε_∞) were held fixed to fit the spectra of the thin films. The dielectric function of the thin films are of the form of a sum of n independent three-parameter damped harmonic oscillators (representing the in-plane polarized TO phonons of the film), which are written as [23]

$$\varepsilon^*(\omega) = \varepsilon_\infty + \sum_{j=1}^{N} \frac{\Delta\varepsilon_j \omega_{TOj}^2}{\omega_{TOj}^2 - \omega^2 + i\omega\gamma_{TOj}}, \quad (3)$$

where $\Delta\varepsilon_j$ is the dielectric strength of the jth mode. Equation (3) is simpler than Eq. (2), but it is well justified because the damping of the LO phonons of the films does not influence the reflectance spectra appreciably.

The THz transmission measurements were performed with a custom-made THz time-domain spectrometer based on a Ti:sapphire femtosecond laser. Linearly polarized THz probing pulses were generated by an interdigitated photoconducting GaAs switch and detected by electro-optic sampling with a 1-mm-thick (110) ZnTe crystal. The in-plane complex dielectric response of the thin films was calculated from the complex THz transmittance and phase spectra measured in an Optistat CF cryostat.

The broadband dielectric properties of the thin-film samples were obtained over a frequency range of 1 kHz to 40 GHz from measurements of an ensemble of planar devices patterned onto the film surface. The devices were lithographically patterned, followed by electron-beam evaporation of a 10-nm-thick titanium adhesion layer followed by a 750-nm-thick gold electrode layer. Lift-off was then performed to complete the structures. Details pertaining to the geometry and device lengths are provided in Ref. [18]. Below 100 MHz, the admittance of interdigitated capacitors (IDCs) of different lengths was measured with a combination of an LCR meter (from 1 kHz to 1 MHz) and a radiofrequency vector network analyzer (from 1 to 100 MHz). From both frequency regimes, we extracted the series capacitance and conductance between the interdigitated fingers. We fit the series capacitance and conductance as a function of the overlap between the interdigitated fingers. We then obtained the distributed capacitance and conductance per unit length for the IDC device directly from the slope. For the high frequency measurement between 100 MHz and 40 GHz, we used the multiline thru-reflect-line algorithm [25,26] to extract the capacitance and conductance per unit length as a function of frequency for the coplanar waveguide device geometry [27,28]. For the measurement between 1 kHz and 40 GHz, we used on-wafer error correction, using a custom calibration standard fabricated on a reference wafer [27].

We performed first principles density functional theory calculations of phonons using the projector augmented wave formalism as implemented in Vienna *Ab initio* Simulation Package (VASP) [29–31]. The equivalent of a Γ-centered $8 \times 8 \times 8$ k-point grid was used for the primitive perovskite cell in all the calculations, along with a plane-wave energy cutoff of 500 eV. The exchange correlation energy was approximated with the Perdew-Burke-Ernzerhof functional PBEsol [32,33].

III. RESULTS AND DISCUSSION

A. Phonon changes with temperature

At room temperature, the (110) $DyScO_3$ substrate has an average in-plane pseudocubic lattice constant of 3.949 Å [34], which provides biaxial tensile strain in $Sr_{n+1}Ti_nO_{3n+1}$ thin films. The lattice mismatch between the film and $DyScO_3$ substrate of the whole series of RP-n compound decreases with n, and therefore the induced tensile strain also decreases as of the films are commensurate: 1.8% for $n = 1$ and 1.1% for $n = \infty$. Details of the film growth, film quality, and evidence that the films were strained commensurately to the underlying substrates may be found elsewhere [18].

We performed IR reflectivity and time domain THz transmission measurements in order to detect the polar phonons and their temperature dependence near the phase transitions. The IR and THz spectra of the thin films were measured in a polarized beam due to the substrate anisotropy. We measured in two IR polarizations $\boldsymbol{E} \parallel [001]$ and $\boldsymbol{E} \parallel [1\bar{1}0]$ with respect to the crystal axes of the (110) $DyScO_3$ substrate. Spectra of

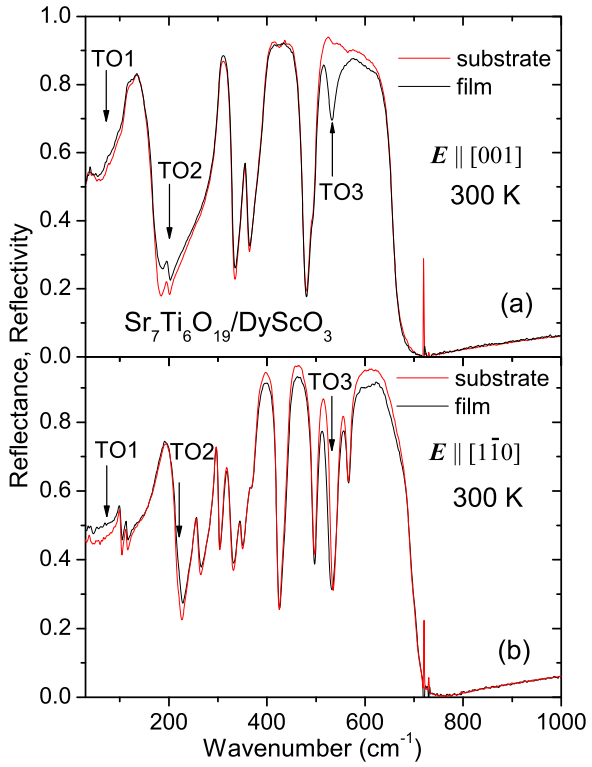

FIG. 2. (Color online) Room-temperature IR reflectivity spectra of $DyScO_3$ substrate and reflectance of the $n = 6$ film deposited on the same substrate. The spectra are taken in polarizations (a) $\boldsymbol{E} \parallel [001]$ and (b) $\boldsymbol{E} \parallel [1\bar{1}0]$ with respect to the substrate crystal axes. The spike near 700 cm^{-1} is caused by a polyethylene polarizer, which is opaque at these frequencies. Frequencies of phonons in thin films are marked.

the substrate and their temperature development correspond to spectra published by Komandin *et al.* [35] or by Lee *et al.* (Supplement of Ref. [36]).

Examples of the room-temperature polarized IR spectra of the substrate and of a strained $Sr_7Ti_6O_{19}$ thin film are shown in Fig. 2. One can see that the signal from the thin film is small compared to the contribution of the substrate, yet it is larger than the measurement sensitivity for our instrumentation, as we will discuss. Thus, the fits on the spectra [following Eqs. (1)–(3)] give reliable parameters of phonons in the films [37]. The strain in the film is isotropic in the plane, and for that reason, the phonon frequencies are the same within the accuracy limits for both polarized spectra. The sensitivity of our spectroscopic method actually depends on the spectral shape (i.e., phonon structure) of the substrate. Sensitivity on phonons in thin films is remarkably enhanced within the restrahlen band of the substrate (i.e., in the frequency range between TO and LO mode frequencies of the substrate) when the TO-LO splitting is large. This is demonstrated in $\boldsymbol{E} \parallel [001]$ polarized spectra [Fig. 2(a)]. The thin-film reflectance spectrum exhibits a minimum in the range between the TO and LO mode frequencies for the substrate (i.e., range $500 - 650$ cm^{-1}). The frequency of the minimum seen at 527 cm^{-1} corresponds exactly to the TO3 phonon frequency (i.e., Axe type mode describing the bending of oxygen octahedra [38]) in the film. In this frequency range, the reflectance spectrum of the thin film deposited on substrate can be roughly understood as transmission spectrum of the film with twice larger film thickness because the substrate reflects very well IR beam between TO and LO frequencies. Note that, in the same spectral range, similar decreases in the reflectance of the film, in comparison with the bare substrate, is seen as well in $\boldsymbol{E} \parallel [1\bar{1}0]$ spectrum [Fig. 2(b)]. Here, no clear minimum is seen due to the rich phonon structure of the substrate. Nevertheless, the fit of the $\boldsymbol{E} \parallel [1\bar{1}0]$ spectrum gives similar TO3 phonon parameters as in the $\boldsymbol{E} \parallel [001]$ spectrum.

The very high sensitivity on the phonons in the thin films is also quantifiable in the spectral range where permittivity of the substrate is low (i.e., reflectivity is low), and where reflectivity of the substrate does not (or weakly) exhibit frequency dependence. This condition is well fulfilled below phonon frequencies (i.e., below 100 cm^{-1}) in $\boldsymbol{E} \parallel [1\bar{1}0]$ spectra and around 200 cm^{-1} in $\boldsymbol{E} \parallel [001]$ spectra (see Fig. 2). For that reason, the best sensitivity on TO1 phonon (Slater-type mode describing mutual Ti-rigid O_6 vibrations [38]) in thin film is in $\boldsymbol{E} \parallel [1\bar{1}0]$ spectra, while the TO2 mode (Last-type mode representing Sr vibrations against the TiO_6-octahedra [38]) is best seen in $\boldsymbol{E} \parallel [001]$ spectra. In both cases, we see enhanced reflectivity in the region of TO1 and TO2 frequencies (Fig. 2). In this paper, we present mainly $\boldsymbol{E} \parallel [1\bar{1}0]$ polarized spectra because the low-frequency phonons (i.e., split TO1 modes) have the highest contributions to permittivity, and they exhibit the largest changes with temperature (i.e., they are responsible together with CM for dielectric anomalies near T_C). The hard TO2 and TO3 modes have only small $\Delta\varepsilon_j$, and their parameters change only slightly with temperature (with exception of their damping).

Figure 3(a) shows the far IR $\boldsymbol{E} \parallel [001]$ polarized reflectivity spectra of the bare $DyScO_3$ substrate together with the far IR reflectance spectra of the $Sr_{n+1}Ti_nO_{3n+1}$ ($n = 1$–6) thin films taken at 10 K. Due to limited space in this paper, we do not present detailed temperature dependences of all spectra in all films, rather we show examples of the temperature changes in spectra for just the $Sr_7Ti_6O_{19}$ film (Fig. 4). It shows increase of TO1 mode intensity on cooling towards 200 K, activation of new TO1n mode near 130 cm^{-1} below T_C, no change of TO2 mode frequency and small hardening of TO3 mode frequency (from 527 cm^{-1} at 300 K to 537 cm^{-1} at 10 K) on cooling. We would like to stress, although $DyScO_3$ substrate spectra exhibit only small change with temperature (see Extended Data Fig. 6(a) in Ref. [36], where only the reflection band near 180 cm^{-1} splits and damping of all modes decreases on cooling), we see clear activation of a new reflection band near 130 cm^{-1} in $Sr_7Ti_6O_{19}$ film (Fig. 4).

In Figs. 3(b) and 3(c), we show the low-frequency real and imaginary parts of the complex permittivity spectra of each of the $n = 1$ to 6 thin films obtained from fits at various temperatures. The $\varepsilon^*(\omega)$ spectra above 300 cm^{-1} were only slightly temperature dependent (data not shown). The in-plane polarized polar phonon frequencies of the $Sr_{n+1}Ti_nO_{3n+1}$ films occur at frequencies of the peaks in $\varepsilon''(\omega)$. We also measured the THz spectra of the $n = 5,6$ samples below 300 K. Due to the magnitude of ε' and ε'' and the thickness of the films, we were not able to detect a THz signal for the films with $n \leqslant 4$. For $n \geqslant 5$, the complex permittivity was large enough to provide sufficient signal-to-noise to extract the dielectric properties in the THz regime. For these films, we observed a broad dielectric

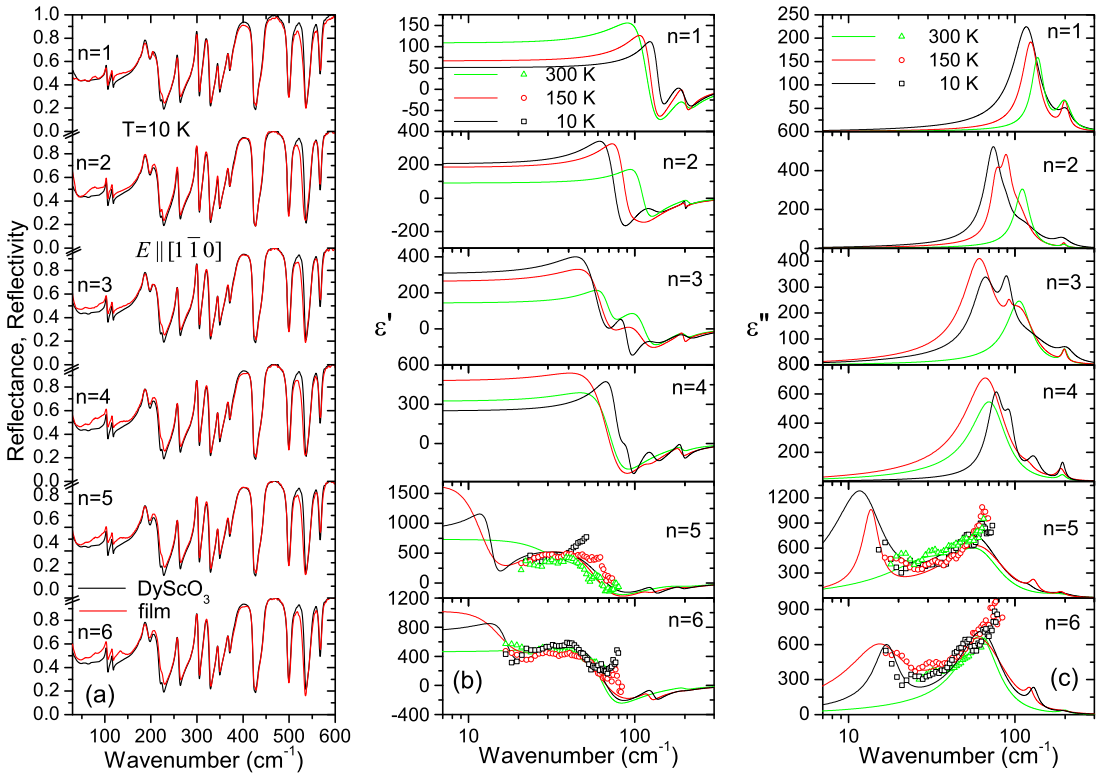

FIG. 3. (Color online) (a) IR reflectance spectra of $n = 1$–6 $Sr_{n+1}Ti_nO_{3n+1}/DyScO_3$ samples taken at 10 K. These spectra are compared with the IR reflectivity spectra of a bare $DyScO_3$ substrate at 10 K. The IR spectra were measured in a polarized beam with $\boldsymbol{E} \parallel [1\bar{1}0]$ with respect to the crystallographic axes of the substrate; (b) real and (c) imaginary parts of the complex permittivity of $n = 1$–6 $Sr_{n+1}Ti_nO_{3n+1}$ films calculated from fits of the IR reflectance spectra at 10, 150, and 300 K.

relaxation below the SM that is attributed to the CM. We fit the CM as an overdamped oscillator with $\gamma_{TO} > \omega_{TO}$. In this case, the dielectric relaxation frequency ω_R corresponds again to the frequency of the peak in $\varepsilon''(\omega)$ and ω_R can be calculated as $\omega_R = \omega_{TO}^2/\gamma_{TO}$. For $n = 5$ sample, the dielectric relaxation is present in the THz regime at all temperatures. In contrast, in the $n = 6$ sample, the dielectric relaxation is seen only below 275 K. Figure 3(c) shows mainly the TO1 phonon response, which has the highest frequency for the $n = 1$ sample. As the number of perovskite layers n becomes greater, the TO1 phonon frequency decreases in frequency, becoming unstable at low temperatures. The resulting phonon splits as the film changes its crystal symmetry.

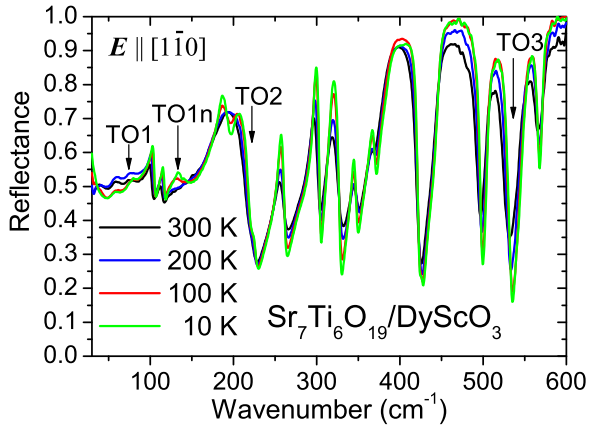

FIG. 4. (Color online) $\boldsymbol{E} \parallel [1\bar{1}0]$ polarized far IR reflectance spectra of $Sr_7Ti_6O_{19}$ film shown at selected temperatures.

To help interpret our experimental results, we used first principles density functional theory calculations to calculate the phonon frequencies of $Sr_{n+1}Ti_nO_{3n+1}/DyScO_3$ with $n = 1 - 6$. The structures are obtained by fixing the in-plane lattice constant a to the theoretical lattice constant of cubic $SrTiO_3$ scaled by +1.1%, simulating the effect of the $DyScO_3$ substrate. We then relaxed the ionic positions and the out-of-plane lattice constant c to minimize the energy. The lowest energy was obtained for a FE polarization along the $[1\bar{1}0]$ axis for all of the RP films. Phonon frequencies were calculated in these FE structures by the direct method. In the FE phase, we found that there were A_1 and B_1 symmetries (irreducible representations of phonons whose eigenvectors lie in the plane of the film). Here, A_1 symmetry modes involved polar vibrations of the ions in the direction parallel to that of the spontaneous FE polarization ($\mathbf{P}_s$), and B_1 polar modes were perpendicular to the $\mathbf{P}_s$. Table I shows the number of optical phonons obtained from group theory for the $n = 1$–6 films. Their theoretical frequencies are listed together with the experimental values in Supplemental Material Table I [39]. Note that we calculated the modes in the strained FE $n = 2$ phase even though we did not observe the FE phase transition for these strained films. The reason that the theoretical calculations obtained a slightly unstable SM (i.e., negative frequency) for the strained $n = 2$ RP films is because quantum fluctuations are not taken into account in the density function theory calculations.

TABLE I. Total number of in-plane polarized polar optical phonons with A_1 and B_1 symmetry expected from theory in FE phases of $Sr_{n+1}Ti_nO_{3n+1}$ ($n = 1-6$) deposited on $DyScO_3$. Strained Sr_2TiO_4 is actually paraelectric at all temperatures and 4 E_u optical phonons are expected in thin film. Out-of-plane polarized phonons are not listed here because they cannot be activated in our near-normal reflectance spectra.

	A_1	B_1
Sr_2TiO_4	6	4
$Sr_3Ti_2O_7$	10	7
$Sr_4Ti_3O_{10}$	15	10
$Sr_5Ti_4O_{13}$	19	13
$Sr_6Ti_5O_{16}$	24	16
$Sr_7Ti_6O_{19}$	28	19

Even though our IR technique had limited sensitivity to weak or overlapping polar modes, the number of optical phonons with A_1 and B_1 symmetries for the $n = 1$–6 films was found to be consistent between first principles calculations and experiment; fewer phonons were seen in experiment than predicted by theory because some modes are weak or overlapped. Strong reflection bands in the substrate above 300 cm^{-1} also limited our sensitivity and ability to model the high-frequency phonons. The temperature dependence of the phonon frequencies below 140 cm^{-1} is shown in Figs. 5(a) and 5(b). The remaining high frequency phonons did not exhibit noticeable temperature dependence (as shown by their frequencies in Supplemental Material Table I [39]).

Three phonons were observed in the Sr_2TiO_4 ($n = 1$) film. Two modes seen at 203 and 535 cm^{-1} exhibit no significant changes with temperature; however, the lowest frequency phonon softens on cooling from 140 cm^{-1} (300 K) down to 120 cm^{-1} (10 K). Consequently, the static permittivity $\varepsilon'(0)$ increases on cooling [Fig. 5(c)] in agreement with the Lyddane-Sachs-Teller relation [40]

$$\frac{\varepsilon'(0)}{\varepsilon_\infty} = \prod_j \frac{\omega_{LOj}^2}{\omega_{TOj}^2}, \tag{4}$$

relating static $\varepsilon'(0)$ and high-frequency ε_∞ permittivity with TO and LO phonon frequencies. In the case of the $n = 2$ film, four modes were detected in the IR spectra (see Supplemental Material Table I [39]), and two of them are seen in Fig. 5(a). Since both modes have lower frequencies than the TO1 mode in the $n = 1$ film, their dielectric strength $\Delta\varepsilon$ is higher than in $n = 1$, and therefore also the static permittivity $\varepsilon'(0)$ is approximately twice as high in the $n = 2$ film than in the $n = 1$ film. The lowest frequency phonon again softens on cooling, and therefore $\varepsilon'(0)$ increases on cooling too [see Fig. 5(c)]. The second mode in the $n = 2$ film significantly hardens below 50 K, but no signature of the phase transitions is seen in the temperature dependence of ε' or in SHG [18]. If the number of perovskite layers increases further to $n = 3$, then we see the instability of the TO1 mode becoming much softer and eventually splitting near 125 K [see green lines in Fig. 5(a)], and therefore a peak appears in $\varepsilon'(T)$ near 125 K [Fig. 5(c)]. Note that an SHG signal was detected below 150 K in the $n = 3$ film [18], suggesting the loss of inversion symmetry which is necessary for FE order. The resulting T_C from SHG and IR spectra agree to within the measurement uncertainty, but polar clusters above T_C may contribute to the small discrepancy.

In the sample with $n = 4$, the T_C is shifted to higher temperature near 175 K. The soft mode exhibits a minimum near this temperature, and two additional modes are activated below T_C [see Fig. 5(a)]. The sum of the phonon contributions to $\varepsilon'(0)$ exhibits a maximum near 175 K, and its value is higher than in the samples with $n \leqslant 3$ [Fig. 5(c)]. Nevertheless,

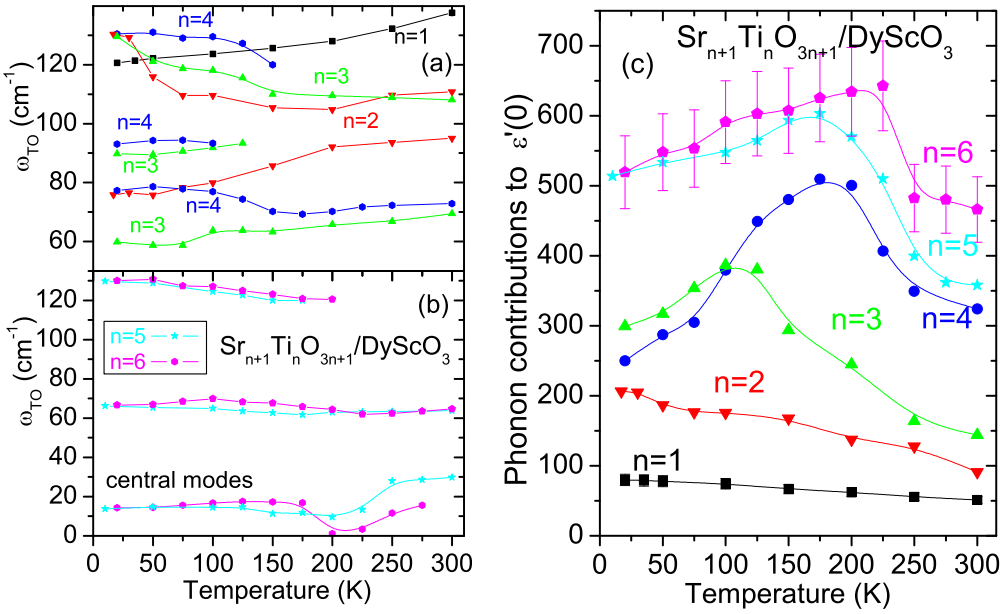

FIG. 5. (Color online) Temperature dependence of the TO phonon and CM frequencies for (a) $n = 1-4$ and (b) $n = 5$ and 6 $Sr_{n+1}Ti_nO_{3n+1}$ films seen below 140 cm^{-1}. (c) Temperature dependence of the total phonon contributions to the static permittivity in each $Sr_{n+1}Ti_nO_{3n+1}$ film. Error bars ±10% of $\varepsilon'(0)$ are shown for $n = 6$. The same error bars ±10% should be by all curves, but for $n = 1$, they are already smaller than the data symbols.

$\varepsilon'(0)$ calculated from the IR spectra is still much smaller than experimental values in the radiofrequency region [Fig. 1(b)]. This is caused by a CM, which contributes to $\varepsilon'(0)$ at frequencies below those of the phonons; it is also responsible for the dielectric dispersion seen in $\varepsilon'(T)$ around T_C.

Not only the CMs are observable in the THz spectra of the films with $n = 5$ and 6 films, but the CMs significantly enhance ε' and ε'' below 30 cm^{-1} [see Figs. 3(b) and 3(c)] and cause the lowest frequency phonon seen near 70 cm^{-1} to become almost temperature independent. In the case of the $n = 5$ film, the CM frequency exhibits a minimal value near 200 K, and an additional phonon activates near 120 cm^{-1} at 175 K. Both effects result in the peak of $\varepsilon'(T)$ near 175 K typical for a FE phase transition [Fig. 5(c)]. We note that the SHG signal appears below 225 K in the $n = 5$ film [18] (i.e., above T_C), indicative of the loss of a center of symmetry (which would be consistent with the formation of polar nanoclusters) below 225 K. From Fig. 5(b), the CM is already active at 300 K, suggesting that the CM is not dependent on the existence of polar nanoclusters, but is rather an independent phenomenon in the $n = 5$ and $n = 6$ strained $Sr_{n+1}Ti_nO_{3n+1}$ thin films.

In the $n = 6$ film, the CM exhibits a minimal frequency already at 200 K [see Fig. 5(b)]. At that temperature, a new phonon near 120 cm^{-1} is activated, and the sum of the phonon contributions to $\varepsilon'(T)$ exhibits a maximum. This is a signature of the FE phase transition near 200 K in the $n = 6$ film. Note that the radiofrequency (RF) $\varepsilon'(T)$ shows a maximum only near 180 K [see Fig. 1(b)]. This is caused by a broad CM, which smears the dielectric anomaly and causes its relaxorlike shape. Note as well that the RF $\varepsilon'(T)$ exhibits a peak that is almost three times higher than ε' calculated from the phonon contributions. Nevertheless, at room temperature, the RF value of ε' is the same as the phonon contribution to $\varepsilon'(0)$, i.e., the CM does not exist at 300 K in the $n = 6$ film. This fact is important in the explanation of the anomalously low MW dielectric loss in the $n = 6$ film, as described below.

B. Central mode and its influence on MW permittivity and loss

To help understand the origin of the CMs near the FE phase transitions, it is useful to consider a displacive FE phase transition driven entirely by soft polar phonons. This can be understood from the Lyddane-Sachs-Teller relation [Eq. (4)] where $\varepsilon'(0)$ diverges at T_C (i.e., the Curie-Weiss Law [23]) as ω_{TO} approaches zero. In practice, the phonon only partially softens, leading to additional dielectric relaxation at lower phonon frequencies as it continues to soften towards T_C. Such excitation was named the CM, since it was first observed in inelastic light and neutron scattering as a central (quasielastic) peak in the spectra [41]. The strength of the relaxation, $S_R = \Delta\varepsilon_R\omega_R$ ($\Delta\varepsilon_R$ – dielectric strength, ω_R – relaxation frequency), follows the sum rules, and if it is not coupled with phonons, S_R is temperature independent [42]. In other words, reduction (frequently called slowing down) of ω_R near T_C causes an increase of $\Delta\varepsilon_R$, and therefore the static permittivity $\varepsilon'(0)$ rises on approaching T_C from above. Below T_C, ω_R increases on cooling and therefore $\varepsilon'(0)$ decreases on cooling. The CM usually appears in the THz or MW frequency region and also slows down again only partially. For that reason $\varepsilon'(T)$ never diverges at T_C, but acquires large, finite values at T_C.

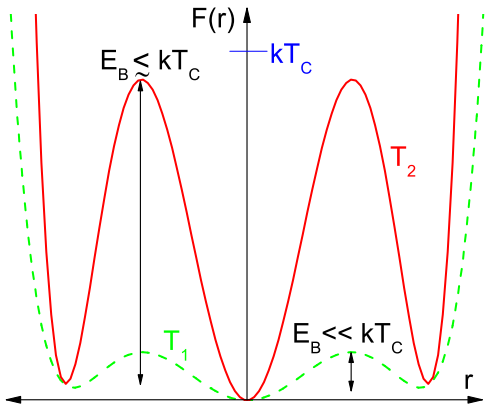

FIG. 6. (Color online) Schematic showing the thermodynamic potential $F(r)$ as a function of displacement r of a FE active cation (e.g. Ti in an RP phase) in the paraelectric phase of a displacive FE at temperature T_1 much higher than T_C (where only the SM contributes to the dielectric dispersion) and at temperature T_2 just above T_C, where both the SM and the CM contribute to $\varepsilon^*(\omega)$.

The influence of the CM on the dielectric spectra of displacive ferroelectrics was reviewed in Refs. [43,44].

In a paraelectric phase far above T_C, the potential landscape is harmonic, and atoms vibrate with frequency ω_{TOj} in a single potential minima or in a quasiharmonic potential with barriers $E_B \ll kT_C$, where k denotes Boltzmann's constant (Fig. 6). In contrast, slightly above a FE phase transition temperature T_C, the potential becomes strongly anharmonic with two or more equivalent minima separated by energy barriers comparable (but less than) to kT_C. When this occurs, the cations not only vibrate with frequency ω_{TOj}, but they also dynamically fluctuate among the equivalent potential minima [7]. The CM simply expresses a dynamical hopping of cations among more equivalent positions. Since the CM frequency ω_R usually lies in the THz and MW region, it can significantly enhance the MW dielectric loss.

As mentioned above, tunable MW dielectrics are usually used in their paraelectric state near T_C because, in this case, ε' is large, can be tuned considerably with an electric field, and dielectric loss is not affected by FE domain wall vibrations. Nevertheless, the CM deteriorates the MW losses, and the question arises: Is there a way to somehow reduce the contribution of the CM to dielectric loss? The CM has intrinsic origin (anharmonicity of the crystal lattice near T_C), but defects can significantly enhance its intensity and enlarge the temperature range over which the CM exists.

Let us demonstrate this point by considering stoichiometric $SrTiO_3$ and nonstoichiometric $Sr_{1+x}TiO_{3+\delta}$ ($-0.05 < x < 0.05$) thin films [45]. When strained by 1% in biaxial tension, $SrTiO_3$ thin films exhibit a FE phase transition near 280 K, but nonstoichiometricity strongly influences the value of ε' at T_C. The RF ε' of a strained, stoichiometric $SrTiO_3$ thin film reaches values up to 70 000, and the peak in $\varepsilon'(T)$ does not exhibit frequency dispersion. In contrast, ε' in strained, nonstoichiometric $Sr_{1+x}TiO_{3+\delta}$ films is reduced by an order of magnitude and even worse, the peak in $\varepsilon'(T)$ exhibits significant frequency dispersion reminiscent of relaxor FE behavior [44]. The SM softens to a greater extent in strained,

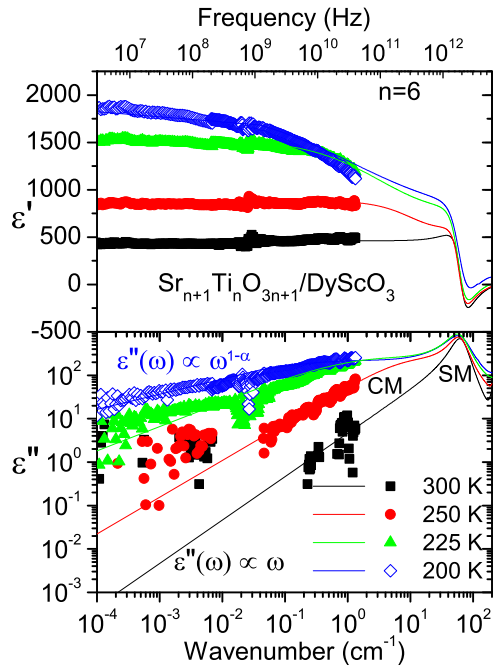

FIG. 7. (Color online) The data points show the frequency dependence of the real and imaginary parts of the complex permittivity of a strained $Sr_7Ti_6O_{19}$ thin film measured at different temperatures from 3 MHz to 40 GHz. The curves show a fit of Eqs. (3) and (5) to the experimental MW and far IR spectra.

stoichiometric $SrTiO_3$ thin films than in nonstoichiometric $Sr_{1+x}TiO_{3+\delta}$, but the SM does not explain the $\varepsilon'(T)$ anomaly at T_C. The CM contribution to $\varepsilon'(T_C)$ is about 90% in the stoichiometric film. An important fact is that, in the stoichiometric film, the CM can be well fitted by a single dielectric relaxation (or overdamped oscillator) in the THz region. Therefore, no relaxor FE dispersion is seen in the RF region. In nonstoichiometric samples, the CM is so broad that it must be expressed by a distribution of Debye relaxations. This results in the frequency dispersion in the RF $\varepsilon'(T)$ near (below and above) T_C and significantly enhances the MW loss far above T_C.

The contribution of the SM and CM to the dielectric permittivity and loss in the strained $n = 6$ RP film is seen in Figs. 5(c) and 7. At room temperature, $\varepsilon'(\omega)$ and $\varepsilon''(\omega)$ are well described by solely phonon contributions, mainly from the SM. This means that $\varepsilon'(\omega)$ is frequency independent below 10 cm^{-1}, and $\varepsilon''(\omega)$ is proportional to ω. At lower frequencies, the CM mode is necessary to explain the MW dielectric dispersion seen in Fig. 7. We tried to fit the CM contribution using an overdamped oscillator or by the Debye relaxation formula, but without success. Experimental MW losses were higher than losses extrapolated from the fits. Only by using a distribution of relaxations expressed by the Cole-Cole formula

$$\varepsilon^*(\omega) = \varepsilon_\infty + \varepsilon_{ph} + \frac{\Delta\varepsilon_R}{1 + i\left(\frac{\omega}{\omega_R}\right)^{1-\alpha}} \qquad (5)$$

we were able to fit the experimental complex dielectric data. Here, $\Delta\varepsilon_R$ and ω_R denote the dielectric strength and mean relaxation frequency of the CM, while the α parameter expresses the distribution of relaxation frequencies. Note that $0 \leqslant \alpha \leqslant 1$; if $\alpha = 0$, Eq. (5) describes a single Debye relaxation. If $\alpha = 0$, the distribution of relaxation frequencies is infinitesimally broad. Here, ε_{ph} in Eq. (5) represents the sum of phonon contributions to permittivity [see Eq. (3)]. The frequency dependence of the MW dielectric loss $\varepsilon''(\omega)$ is proportional to the first power of the frequency ω in the case of only phonon contributions. Such frequency dependence can be obtained from the low-frequency ($\omega \ll \omega_{TO}$) limit of in Eq. (3) [13]. Nevertheless, in the case of the Cole-Cole formula, the MW loss is proportional to $\omega^{1-\alpha}$. In other words, the loss decreases more slowly below ω_R, and therefore in the strained $n = 6$ RP film, the MW losses are higher at low temperatures than at 300 K, where no CM exists. One can also see in Fig. 7 that ε' depends on frequency below ω_R, resulting in the development of a frequency dispersion in $\varepsilon'(T)$ near T_C.

One can see from Fig. 7 that the slope of $\varepsilon''(\omega)$ decreases (MW loss increases) on cooling because α is increasing with lowering temperature. Our fit gives $\alpha = 0.16$ at 250 K and $\alpha = 0.61$ at 200 K. The distribution of relaxation frequencies described by the parameter α can be explained by a distribution of energy barriers E_B among potential minima. If the lattice is perfectly periodic, the potential barriers are always the same (uniform), and dielectric dispersion can be modeled by the Debye formula (i.e., Cole-Cole with $\alpha = 0$). If the value of potential barriers fluctuate, $\alpha \neq 0$ is necessary. An extreme case occurs in FE relaxors below their freezing temperatures T_f, where $\alpha = 1$, i.e. $\varepsilon''(\omega)$ is finite and has a frequency independent value at frequencies from subHz up to THz due to the distribution of energy barriers from zero up to some finite value higher than kT_f [46]. In relaxor FEs (like $PbMg_{1/3}{}^{2+}Nb_{2/3}{}^{5+}O_3$), the distribution of E_B is caused by chemical disorder on the ABO_3 perovskite B sites, which induces random fields [47]. In $Sr_{n+1}Ti_nO_{3n+1}$, the distribution of E_B is likely caused by oxygen vacancies or by the stacking faults frequently presented in RP structures (see Refs. [10,18]). In any case, the CM is an intrinsic feature of all displacive FE phase transitions, it always enhances MW losses, and its influence is further enhanced by defects in the structure. Note that the CM disappears at some temperature above T_C. In $BaTiO_3$, it exists at least 250 K above $T_C = 410$ K [48]; in $Ba_{0.5}Sr_{0.5}TiO_3$, the CM disappears just 150 K above $T_C =$ 245 K [7], and in our strained $Sr_7Ti_6O_{19}$ thin film, the CM is already absent at only 100 K above $T_C \approx 200$ K. This is the main reason that the room-temperature dielectric loss is extremely low in strained $Sr_7Ti_6O_{19}$.

From Fig. 6, one can understand why it is that the temperature range over which the CM exists increases with T_C. The higher the T_C, the higher the value of the barrier E_B, resulting in a lattice that is more anharmonic over a broader temperature range above T_C. Simultaneously, one cannot claim that the temperature range where CM exists corresponds to the temperature range where polar nanoclusters and SHG signal exist. The CM can exist over a broader temperature range than the polar clusters. For example, in $BaTiO_3$, the polar clusters and SHG signal disappear just ~70 K above T_C [49], while the CM exists 250 K above T_C [45]. Nevertheless, if the occurrence of the CM is proportional to T_C, the CM should be absent in the strained $n = 5$ RP film at 300 K, which is not true, despite of its lower $T_C \approx 175$ K than the $n = 6$ film.

The room-temperature MW loss in the strained $n = 5$ RP film is higher than in the strained $n = 6$ RP film. This is probably caused by higher concentration of defects in the $n = 5$ RP film. This hypothesis is also qualitatively supported by the SHG results in Ref. [18]. The SHG signal appears at a higher temperature in the strained $n = 5$ film than in the strained $n = 6$ film, signifying that the center of space symmetry is lost at a higher temperature in the former than in the latter film. We note that our strained RP films contain high concentrations of stacking faults, which we believe to be a way in which the films can accommodate local nonstoichiometry. These stacking faults give rise to the inclusion of perovskite blocks containing more than n perovskite layers, e.g., commonly with $2n$, $3n$, $4n$, etc., numbers that are well lattice matched to the surrounding matrix [50]. Specifically, the strained $n = 6$ RP film was observed to contain stacking faults with $n = 12$, 18, 24 inclusions [18], which would be expected to have higher T_C than the strained $n = 6$ film, but a lower T_C than strained $SrTiO_3$ ($n = \infty$) films ($T_C = 280$ K). Simultaneously, these inclusions would be expected to have higher ε' than strained $n = 6$ films.

We end by briefly discussing the tunability of the permittivity through the application of an electric field in strained RP films. ε' is enhanced by strain in the RP films, and the tunability is caused by a sensitivity of both the CM and SM frequency to the applied electric field. This was directly seen in strained $SrTiO_3$ films [16]. In the strained $n = 6$ RP film, the CM is absent at room temperature. The tunability of ε' by an electric field should thus only be caused by the ability to tune the SM frequency. Nevertheless, because of the low dielectric loss at 300 K, the figure of merit of the strained $n = 6$ RP film rivals all known MW dielectrics.

IV. CONCLUSIONS

Although biaxially strained $Sr_{n+1}Ti_nO_{3n+1}$ (n = 3–6) thin films deposited on $DyScO_3$ substrates exhibit relaxor-like dielectric anomalies near the maxima of $\varepsilon'(T)$, our IR reflectance spectra clearly reveal phonon and central mode anomalies typical of structural phase transitions. Since studies on these same films reveal SHG signal and polarization hysteresis loops below T_{max} [18], we can conclude that the $Sr_{n+1}Ti_nO_{3n+1}/DyScO_3$ films are FE for $n \geq 3$. Detailed analysis of the MW, THz, and IR spectra of a strained $Sr_7Ti_6O_{19}$ thin film revealed the presence of a central mode below 275 K, which drives the FE phase transition and is responsible for rather high MW loss. The CM disappears at 300 K, resulting in the MW loss being extremely low. This fact, together with the high tunability of this strained $Sr_7Ti_6O_{19}$ film [18], is responsible for the extremely high figure of merit in this material. General conditions for the activation of the CMs near FE phase transitions are discussed in detail. It is shown that, although a high tunability of ε' by an applied electric field can be expected near T_C, a high figure of merit (i.e., low MW loss) at room temperature can only be obtained in systems where the CM becomes absent at room temperature. This can be expected in materials whose critical temperatures will be near or below 200 K and which will have simultaneously low concentration of defects. A system where such behavior might also be seen is 0.6% tensile strained $SrTiO_3$ film deposited on a $Sr_{2.06}Al_{0.24}Ga_{0.70}TaO_{5.96}$ substrate, provided the concentration of defects in the $SrTiO_3$ film can be kept sufficiently low.

ACKNOWLEDGMENTS

This paper was supported by the Czech Science Foundation Project No. P204/12/1163 and the Czech Ministry of Education, Youth and Sports, Project No. LH13048. The work at Cornell was supported by the Army Research Office (ARO) Grant No. W911NF-12-1-0437. The MW measurements are an official contribution of the National Institute of Standards and Technology (NIST); not subject to copyright in the United States. Description of commercial products herein is for information only; it does not imply recommendation or endorsement by the NIST.

[1] A. K. Tagantsev, V. O. Sherman, K. F. Astafiev, J. Venkatesh, and N. Setter, J. Electroceram. **11**, 5 (2003).
[2] S. Gevorgian, *Ferroelectrics in Microwave devices, Circuits and Systems* (Springer-Verlag, London Limited 2009).
[3] V. V. Lemanov, E. P. Smirnova, P. P. Syrnikov, and E. A. Tarakanov, Phys. Rev. B **54**, 3151 (1996).
[4] P. Bao, T. J. Jackson, X. Wang, and M. J. Lancaster, J. Phys. D: Appl. Phys. **41**, 063001 (2008).
[5] A. Kozyrev, V. Keis, V. Osadchy, A. Pavlov, O. Buslov, and L. Sengupta, Integr. Ferroelectrics **34**, 189 (2001).
[6] J. C. Booth, I. Takeuchi, and K. S. Chang, Appl. Phys. Lett. **87**, 082908 (2005).
[7] J. Weerasinghe, L. Bellaich, T. Ostapchuk, P. Kužel, C. Kadlec, S. Lisenkov, I. Ponomareva, and J. Hlinka, MRS Commun. **3**, 41 (2013).
[8] S. N. Ruddlesden and P. Popper, Acta Crystallogr. **10**, 538 (1957).
[9] S. N. Ruddlesden and P. Popper, Acta Crystallogr. **11**, 54 (1958).
[10] P. L. Wise, I. M. Reaney, W. E. Lee, T. J. Price, D. M. Iddles, and D. S. Cannell, J. Eur. Ceram. Soc. **21**, 1723 (2001).
[11] D. Noujni, S. Kamba, A. Pashkin, V. Bovtun, J. Petzelt, A.-K. Axelsson, N. McNAlford, P. L. Wise, and I. M. Reaney, Integr. Ferroelectrics **62**, 199 (2004).
[12] N. D. Orloff, W. Tian, C. J. Fennie, C. H. Lee, D. Gu, J. Mateu, X. X. Xi, K. M. Rabe, D. G. Schlom, I. Takeuchi, and J. C. Booth, Appl. Phys. Lett. **94**, 042908 (2009).
[13] S. Kamba, P. Samoukhina, F. Kadlec, J. Pokorny, J. Petzelt, I. M. Reaney, and P. L. Wise, J. Eur. Ceram. Soc. **23**, 2639 (2003).
[14] K. A. Müller and H. Burkard, Phys. Rev. B, **19**, 3593 (1979).
[15] J. H. Haeni, P. Irvin, W. Chang, R. Uecker, P. Reiche, J. L. Li, S. Choudhury, W. Tian, M. E. Hawley, B. Craigo, A. K. Tagantsev, X. Q. Pan, S. K. Streiffer, L. Q. Chen, S. W. Kirchoefer, J. Levy, and D. G. Schlom, Nature **430**, 758 (2004).

[16] C. Kadlec, V. Skoromets, F. Kadlec, H. Němec, J. Hlinka, J. Schubert, G. Panaitov, and P. Kužel, Phys. Rev. B **80**, 174116 (2009).

[17] T. Birol, N. A. Benedek, and C. Fennie, Phys. Rev. Lett. **107**, 257602 (2011).

[18] C. H. Lee, N. D. Orloff, T. Birol, Y. Zhu, V. Goian, E. Rocas, R. Haislmaier, E. Vlahos, J. A. Mundy, L. F. Kourkoutis, Y. Nie, M. D. Biegalsky, J. Zhang, M. Bernhagen, N. A. Benedek, Y. Kim, J. D. Brock, R. Uecker, X. X. Xi, V. Gopalan *et al.*, Nature (London) **502**, 532 (2013).

[19] R. Uecker, B. Velickov, D. Klimm, R. Bertram, M. Bernhagen, M. Rabe, M. Albrecht, R. Fornari, and D. G. Schlom, J. Cryst. Growth **310**, 2649 (2008).

[20] C. D. Theis and D. G. Schlom, J. Vac. Sci. Technol. A **14**, 2677 (1996).

[21] J. H. Haeni, C. D. Theis, and D. G. Schlom, J. Electroceram. **4**, 385 (2000).

[22] V. Železný, I. Fedorov, and J. Petzelt, Czech J. Phys. **48**, 537 (1998).

[23] F. Gervais, *Infrared and Millimeter Waves*, edited byK. J. Button (Academic, New York, 1983), Vol. 8, Chap. 7, p. 279.

[24] M. Rössle, C. N. Wang, P. Marsik, M. Yazdi-Rizi, K. W. Kim, A. Dubroka, I. Marozau, C. W. Schneider, J. Humlíček, D. Baeriswyl, and C. Bernhard, Phys. Rev. B **88**, 104110 (2013).

[25] R. B. Marks, IEEE Trans. Microw. Theory Tech. **39**, 1205 (1991).

[26] D. F. Williams, J. C. M Wang, and U. Arz, IEEE Trans. Microw. Theory Tech. **51**, 2391 (2003).

[27] N. D. Orloff, J. Mateu, A. Lewandowski, E. Rocas, J. King, G. Dazhen, X. Lu, C. Collado, I. Takeuchi, and J. C. Booth, IEEE Trans. Microw. Theory Tech. **59**, 188 (2011).

[28] N. Orloff, J. Mateu, M. Murakami, I. Takeuchi, and J. C. Booth, in *Proceedings of IEEE MTT-S International Microwave Symposium* (IEEE, Piscataway, NJ, 2007), p. 1177.

[29] P. E. Blochl, Phys. Rev B **50**, 17953 (1994).

[30] G. Kresse and D. Joubert, Phys. Rev. B **59**, 1758 (1999).

[31] G. Kresse and J. Furthmuller, Comput. Mater. Sci. **6**, 15 (1996).

[32] J. P. Perdew, K. Burke, and M. Ernzerhof, Phys. Rev. Lett. **77**, 3865 (1996).

[33] J. P. Perdew, A. Ruzsinszky, G. I. Csonka, O. A. Vydrov, G. E. Scuseria, L. A. Constantin, X. Zhou, and K. Burke, Phys. Rev. Lett. **100**, 136406 (2008).

[34] B. Velickov, V. Kahlenberg, R. Bertram, and M. Bernhagen, Z. Kristallogr. **222**, 466 (2007).

[35] G. A. Komandin, E. S. Zhukova, V. I. Torgashev, A. V. Boris, E. A. Motovilova, A. S. Prokhorov, L. S. Kadyrov, B. P. Gorshunov, and M. Dressel, J. Appl. Phys. **114**, 024102 (2013).

[36] J. H. Lee, L. Fang, E. Vlahos, X. Ke, Y. W. Jung, L. Fitting Kourkoutis, J.-W. Kim, P. J. Ryan, T. Heeg, M. Roeckerath, V. Goian, M. Bernhagen, R. Uecker, P. Ch. Hammel, K. M. Rabe, S. Kamba, J. Schubert, J. W. Freeland, D. A. Muller, C. J. Fennie *et al.*, Nature **466**, 954 (2010).

[37] Room-temperature spectra were measured up to 4000 cm^{-1}. It allowed us to determine ε_∞ of the substrate, but the middle IR spectrum of the thin film has the same reflectance as the substrate, because ε_∞ of the film and substrate ($\varepsilon_\infty = 3.4$) are comparable. In our case, we took ε_∞ of films same as in $Sr_{n+1}Ti_nO_{3n+1}$ ceramics known from Refs. [11,13] ($\varepsilon_\infty = 5.4 - 5.8$ in dependence of n, note that $SrTiO_3$ has $\varepsilon_\infty = 5.8$). Possible small change of ε_∞ with strain can have only negligible influence on phonon parameters.

[38] J. Hlinka, J. Petzelt, S. Kamba, D. Noujni, and T. Ostapchuk, Phase Transitions **79**, 41 (2006).

[39] See Supplemental Material at http://link.aps.org/supplemental/10.1103/PhysRevB.90.174105 for comparison of experimental and theoretical phonon frequencies.

[40] R. H. Lyddane, R. G. Sachs, and E. Teller, Phys. Rev. **59**, 673 (1941).

[41] A. D. Bruce and R. A. Cowley, Advances in Physics **29**, 219 (1980).

[42] In practical cases, the CM is always coupled with the SM and receives its strength from the SM. For that reason, both dielectric strength $\Delta\varepsilon_R$ and strength of relaxation S_R increase on cooling towards T_C. See Refs. [7,16] for further details.

[43] J. Petzelt, G. V. Kozlov, and A. A. Volkov, Ferroelectrics **73**, 101 (1987).

[44] E. Buixaderas, S. Kamba, and J. Petzelt, Ferroelectrics **308**, 131 (2004).

[45] C.-H. Lee, V. Skoromets, M. D. Biegalski, S. Lei, R. Haislmaier, M. Bernhagen, R. Uecker, X. Xi, V. Gopalan, X. Marti, S. Kamba, P. Kužel, and D. G. Schlom, Appl. Phys. Lett. **102**, 082905 (2013).

[46] I. Rychetský, S. Kamba, V. Porokhonskyy, A. Pashkin, M. Savinov, V. Bovtun, J. Petzelt, M. Kosec, and M. Dressel, J. Phys.: Condens. Matter **15**, 6017 (2003).

[47] V. Westphal, W. Kleemann, and M. D. Glinchuk, Phys. Rev. Lett. **68**, 847 (1992).

[48] I. Ponomareva, L. Bellaiche, T. Ostapchuk, J. Hlinka, and J. Petzelt, Phys. Rev. B **77**, 012102 (2008).

[49] E. Dul'kin, J. Petzelt, S. Kamba, E. Mojaev, and M. Roth, Appl. Phys. Lett. **97**, 032903 (2010).

[50] W. Tian, X. Q. Pan, J. H. Haeni, and D. G. Schlom, J. Mat. Research **16**, 2013 (2001).